New Journal of Physics
The open-access journal for physics

Crash and recovery of the potential in a toroidal plasma column, as observed by generalized conditional sampling

Å Fredriksen[1], H L Pécseli[2,4] and J Trulsen[3]

[1] University of Tromsø, Department of Physics and Mathematics, N-9037 Tromsø, Norway
[2] University of Oslo, Physics Department, PO Box 1048 Blindern, N-0316 Oslo, Norway
[3] University of Oslo, Institute of Theoretical Astrophysics, PO Box 1029 Blindern, N-0315 Oslo, Norway
E-mail: Ashild.Fredriksen@phys.uit.no, hans.pecseli@fys.uio.no and j.k.trulsen@astro.uio.no

New Journal of Physics **10** (2008) 033030 (19pp)
Received 12 November 2007
Published 18 March 2008
Online at http://www.njp.org/
doi:10.1088/1367-2630/10/3/033030

Abstract. Conditional sampling methods are generalized by applying a matched-filter on the reference signal. This generalized method is illustrated by data obtained in a magnetized toroidal plasma without rotational transform. By proper choice of the filter characteristics we can observe a rapid 'crash' in the electrostatic plasma potential in the entire plasma column. The crash is then followed by a slower recovery phase. The results are noticeably different from those found by using a more traditional conditional analysis of the same data. The significant differences between the two results indicate that generalizations of the conditional sampling method can give new insights. Conditionally obtained local power spectra demonstrate an enhancement in the amplitude of the fluctuations preceding the potential crash. The analysis is also illustrated by using a synthetic dataset.

[4] Author to whom any correspondence should be addressed.

Contents

1. Introduction **2**
1.1. Matched filters . . . 3
2. Description of the experiment **4**
2.1. Steady state conditions . . . 4
2.2. Spontaneous fluctuations in the toroidal plasma . . . 5
3. Conditional sampling methods and their generalizations **6**
3.1. Conditional sampling of Gaussian noise . . . 8
4. Methods for data analysis **9**
4.1. Test of the method using synthetic data . . . 10
5. Experimental results **12**
5.1. Conditionally averaged fluctuations . . . 12
5.2. Distribution of events . . . 14
5.3. Conditioned spectra . . . 15
6. Conclusions **16**
Acknowledgments **17**
References **17**

1. Introduction

Conditional sampling methods have been extensively used for studying random fluctuations in fluids [1] and plasmas [2] as well as in other contexts, although there seems to be no consensus on the name of the method (sometimes it is used without any explicit name). In space-plasma studies, for instance, the often used analysis based on 'superposed epochs' [3] is, at closer inspection, very similar to the conditional sampling method. The signal need not be time stationary in a statistical sense, but in practice the ideas are most readily carried out for this case. The complexity of the analysis can change, depending on the nature of the phenomena being investigated: when analyzing fluid turbulence, the full information of the three-dimensional (3D) conditional flow vector can be desired, while for electrostatic plasma fluctuations measurements of a scalar potential will suffice in many cases.

The conditional sampling method as used in the present work has been described in detail elsewhere [2, 4, 5]. Basically, the idea assumes that a signal record is analyzed subject to an *a priori* imposed condition, requiring for instance that the signal takes a prescribed value within a certain interval. Selecting a time interval centered around the reference times, many events fulfilling the condition are subsequently averaged. The analysis can be carried out on the reference signal itself, but more information can be found by analyzing other simultaneously obtained data records. By such a procedure, it is possible to analyze the full space-time variation of, say, the conditioned signal evolution of an entire cross-section of a plasma column. As illustrated elsewhere [2, 5], a significant generalization of the method can be achieved by imposing additional constraints on the sampling condition, for instance a criterion on the sign of the derivative of the signal at the reference time. More elaborate conditions have also been used [5].

In the simplest version of the method, as used in the majority of the works mentioned, the analysis gives emphasis to large amplitude phenomena. It has been demonstrated that the characteristics of the space-time variation of localized burst-like events can be identified under very different experimental conditions [4]–[6]. Seemingly, most investigations have focused on low frequency phenomena in magnetized plasmas, flute modes and drift waves, for instance, but the method as such has much wider applications. Numerical model studies [7] as well as laboratory investigations [8]–[10] have shown that very detailed information can be recovered, although some nontrivial limitations of the method have been pointed out as well [11, 12]. In the case where we have two different structures present with approximately the same characteristic amplitudes, the standard conditional averaging will emphasize the one that occurs most frequently. If the relevant signal is embedded in larger amplitude random noise, the conditional sampling is, in effect, reproducing the properties of this noise.

1.1. Matched filters

Improvements of the conditional sampling method can be obtained by some sort of pre-processing of the data, where the methods used will in general depend on the problem [13]. The conditional sampling method becomes particularly problematic for studies of small amplitude phenomena embedded in larger amplitude noise. In the present study we illustrate how that type of problem can be analyzed by use of a matched filter [14, 15] together with some given (or assumed) *a priori* knowledge. Assuming that a repetitive, but otherwise randomly occurring, deterministic structure $w(t-t_j)$ centered around some time t_j is present in the signal, we attempt to devise a linear filter detecting this structure. We let a reference (scalar) signal be $I(t) = h(t) + w(t-t_j)$, with $h(t)$ being an additive noise component, independent of the presence of w. For the case where h is white noise, the signal-to-noise ratio of the filter output is defined as

$$\frac{\mathcal{S}}{\mathcal{N}} \equiv \frac{\left(\int_{-\infty}^{\infty} f(\tau)w(t-\tau)\,\mathrm{d}\tau\right)^2}{\sigma_n^2 \int_{-\infty}^{\infty} f^2(\tau)\,\mathrm{d}\tau}, \tag{1}$$

where $f(\tau)$ is the filter impulse response and σ_n^2 the noise power per unit of the frequency interval $\{-\infty;\infty\}$. For the case where h is white noise, the optimum filter response that maximizes $\mathcal{S}/\mathcal{N}$ is evidently $f(\tau) = w(t-\tau)$, i.e. the waveform 'running backwards'. The filter obtained this way is optimum for white noise, but can be used with confidence in cases where the Fourier spectrum of the noise covers a frequency range that is much wider than what is obtained for the structure. The maximum signal-to-noise ratio we can obtain when $h(t)$ represents white noise is

$$\left.\frac{\mathcal{S}}{\mathcal{N}}\right|_{\max} = \frac{1}{\sigma_n^2}\int_{-\infty}^{\infty} w^2(\tau)\,\mathrm{d}\tau.$$

It is important to note that the filter does not reproduce the signal, it merely gives a maximal output at a time where the signal is most likely to be present in the background noise. The discussion of the optimum filter design can be generalized [14], but the present short summary will suffice here.

The paper is organized as follows. In section 2, we present details of the experimental set-up and the plasma conditions. Section 3 discusses the conditional sampling method and its generalization. Section 4 summarizes the methods used, giving details of the matched filter

being used. In section 5, we give the results obtained by the generalized conditional averaging. In particular, we also show the local power spectrum when the imposed condition on the reference signal is fulfilled. Finally, section 6 gives our summary and conclusions.

2. Description of the experiment

We here summarize the diagnostics, the steady state conditions of the plasma and the basic features of the spontaneously excited fluctuations.

2.1. Steady state conditions

The experimental data were obtained in the Blaamann toroidal device at the University of Tromsø, where a magnetized plasma is produced by discharge from a hot filament [16]. In steady state operation, the plasma generated is balanced by losses, although we note that the steady state conditions should here be understood in an averaged sense [16, 17]. The major radius of the torus is $R = 0.67\,\mathrm{m}$ and the minor radius $r_0 = 0.135\,\mathrm{m}$. The plasma forms a negative potential well near the center of the poloidal cross-section and is subject to vertical ∇B and curvature drifts and poloidal $\mathbf{E}\times\mathbf{B}$-drift. The degree of ionization is typically ∼1%. There is no toroidal current nor poloidal magnetic fields imposed on the plasma, and hence no poloidal transform exists. The present experiment [18] was carried out in a helium gas at a pressure of $3.0\times10^{-4}\,\mathrm{mbar}$ and a discharge current of approximately 1 A. The toroidal magnetic field was set to 1.54 kG, and the hot filament was biased at 160 V with respect to the walls. The plasma conditions depend significantly on the imposed potentials and magnetic fields [19, 20].

The hot filament can emit electrons in abundance, and the plasma is electron rich, with a deep negative almost parabolic potential profile. The corresponding radial electric field $E_\mathrm{r} \approx E_0 r/r_0$, gives rise to an almost solid body $\mathbf{E}\times\mathbf{B}$-rotation of the plasma column, since the magnetic field varies only little over the plasma cross-section. In our case $E_0 \approx 10^3\,\mathrm{V\,m^{-1}}$ and $E_0/B_0 \approx 6.5\times10^3\,\mathrm{m\,s^{-1}}$. For comparison we have the ion acoustic sound speed $C_\mathrm{s} = \sqrt{\kappa T_\mathrm{e}/M} \approx 11\times10^3\,\mathrm{m\,s^{-1}}$ for singly charged helium ions. The ion component at a position r experiences a noticeable radial centrifugal force $F = M\Omega^2 r$, with $r_0\Omega \equiv E_0/B_0$, where we here estimate $\Omega/2\pi \approx 7.7\times10^3\,\mathrm{Hz}$. We have gyrofrequencies $\omega_\mathrm{ce} = 2.7\times10^{10}\,\mathrm{s^{-1}}$ for the electrons, and $\omega_\mathrm{ci} = 3.7\times10^6\,\mathrm{s^{-1}}$ for singly charged helium ions at the reference magnetic field value. An often used length scale is $a_\mathrm{i} \equiv C_\mathrm{s}/\omega_\mathrm{ci} \approx 3.1\times10^{-3}\,\mathrm{m}$. A characteristic ion Larmor radius is then $r_\mathrm{L} = a_\mathrm{i}\sqrt{T_\mathrm{i}/T_\mathrm{e}} \approx 1\times10^{-3}\,\mathrm{m}$. An electron Debye length is $\lambda_\mathrm{D} \approx 50\times10^{-6}\,\mathrm{m}$, corresponding to the peak electron density and temperature. The rotating frame of reference where the electric field force balances the centrifugal force on the ions rotating with an angular frequency Ω_+ is determined by

$$\frac{\Omega_+}{|\Omega|} = -\frac{1}{2}\frac{\omega_\mathrm{ci}}{|\Omega|}\left(1 \pm \sqrt{1+4\frac{|\Omega|}{\omega_\mathrm{ci}}}\right).$$

With the ion Larmor radius being smaller than the column radius, $r_\mathrm{L} < r_0$, the relevant solution is here the one corresponding to the minus sign [21]. In the absence of ion–neutral collisions, this would be the rotation frame of the ions, apart from small corrections depending on the relative direction of the ion gyration and the plasma rotation, i.e. the sign of the magnetic field direction for given electric field [21, 22]. For the present case with helium ions, the ratio $|\Omega|/\omega_\mathrm{ci}$

is small, but the correction can be important for heavier ions and smaller magnetic fields, given E_0. Friction with the neutral gas component can be accounted for by a collision frequency $\nu_{i,n}$, which reduces Ω_+ as given by analytical results in the literature [23]. Due to their small mass the electrons experience a negligible centrifugal force, and the friction with the neutral component can also be taken to be small when $\omega_{ce} \gg \nu_{e,n}$, where $\nu_{e,n}$ is the electron neutral collision frequency so that the electron rotation frequency $\Omega_- \approx |\Omega|$. The difference between Ω_- and Ω_+ gives rise to an azimuthal current flow in the plasma, which can be the source of an interchange instability at all azimuthal positions of the plasma.

The probe system used to obtain conditionally sampled data consists of one fixed reference probe placed 4.5 cm above the horizontal mid-plane, and one probe which could scan the entire poloidal cross-section at a toroidal position nearly intersecting that of the reference probe. In the present set-up, 225 positions were used to map the entire plasma cross-section. The scanning probe had three cylindrical probe tips oriented perpendicularly to the magnetic field with 2 mm poloidal distance between them so that each probe tip intercepted different magnetic field lines. Data were acquired from the reference probe and the movable probe simultaneously, with a 2 channel digital oscilloscope (Tektronix 2430), each channel being sampled at 250 kHz, at 4 μs time resolution, with 1024 points for each data record. At each position of the moving probe position, 10 records were acquired, to obtain a total time series of 40.96 ms and 10 240 points per probe position. The electron saturation current and the floating potential were measured with the movable probe, each in separate scans and simultaneously with the floating potential signal from the reference probe. The dc component was removed to obtain the time series of the data used in the analysis. In this experiment, the electron saturation current I_{sat}^- was used to represent the density fluctuations, as it gives basically the same results as we obtained from the ion saturation current from a floating double probe. To obtain the electron saturation current, the probe tip was biased positively at +45 V with respect to ground, and the current was drawn through a 1 kΩ resistor. The floating potential was measured over a 1 MΩ resistor to ground. The electron temperature fluctuations could be measured by a triple probe, with a 36 V bias applied between the floating double-probe tips.

The full cross-section of background dc plasma parameters were obtained by one of the probe tips on the 2D probe being swept between ± 25 V from a dc-level set by batteries to keep it close to the local plasma potential. Peak values of the time averaged densities were $\overline{n} \approx 2 \times 10^{17}$ m^{-3}. Peak electron temperatures were max $\{\overline{T_e}\} \approx 6$ eV and the local minimum of the time averaged plasma potential was $\overline{\phi} \approx -50$ V. In figure 1 we show the dc plasma density, the time averaged potential and the electron temperature for a cross-section of the plasma. The averaged electron temperature is elongated in the vertical direction along the hot filament. The averaged potential profile is less elongated, and is approximately parabolic in the region close to the minimum. The electron density has a local maximum close to the point of maximum electron temperature. The position of average peak density is slightly displaced from the position where the average potential is minimum.

2.2. Spontaneous fluctuations in the toroidal plasma

Low frequency electrostatic fluctuations are excited spontaneously in the toroidal plasma [16, 17] which has been studied experimentally in some detail [24, 25]. A fluctuating component with a well-defined frequency is generally assumed to be an interchange mode [25] where the frequency is determined by the plasma rotation discussed in section 2.1. The plasma rotation

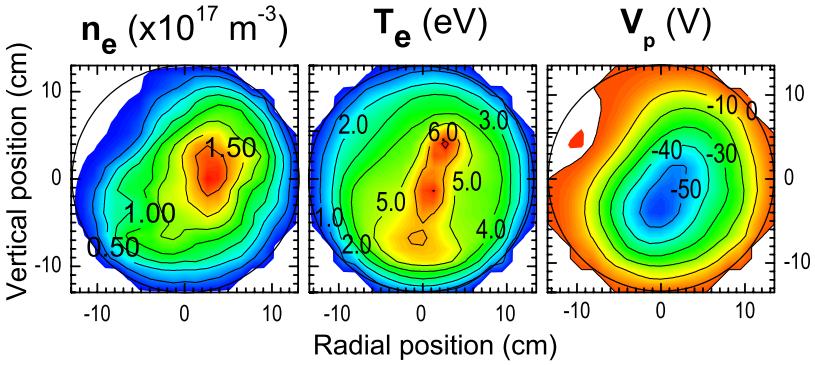

Figure 1. The dc plasma density, the potential and the electron temperature for a cross-section of the plasma. 'Radial direction' refers here to the major radius of the torus. The narrow vertical region of enhanced electron temperature is close to the filament position.

will generally not be entirely uniform, and a shear in the angular rotation can modify the most unstable mode. The role of a Farley–Buneman and the associated gradient drift instability [22, 26, 27] has not been considered in the present context, mainly because these instabilities require the difference between the local electron and ion flow velocities to exceed the sound speed. For larger ion masses and weaker magnetic fields, this instability might become relevant. The potential-relaxation instability [28, 29] has been suggested, since the negatively biased hot filament has a direct contact to the grounded confining vessel along a magnetic field line when a small vertical field component is imposed by external coils. The frequency of the potential relaxation instability is determined by a transit time, i.e. $\omega_t/2\pi \sim C_s/\mathcal{L}$ where $\mathcal{L}$ is the distance between the filament and the vessel, measured along a magnetic field line. Since the vertical externally imposed magnetic field is weak, we have as a distance $\mathcal{L} \gg 2\pi R$, which implies $\omega_t/2\pi \ll 2.6 \times 10^3$ Hz. The period of this relaxation instability depends critically on $\mathcal{L}$, which in turn is very sensitive to the vertical magnetic field.

In figure 2, we show the estimate for the amplitude probability density of the fluctuating potential ϕ as obtained by the reference probe for the present conditions. We find a slightly negative skewness, $S \equiv \langle(\phi - \langle\phi\rangle)^3\rangle/\sigma^3 \approx -0.07$, where σ is the standard deviation. The signal is leptokurtic by having a positive kurtosis as compared to the reference value for Gaussian signals, $K \equiv \langle(\phi - \langle\phi\rangle)^4\rangle/\sigma^4 - 3 \approx 0.24$.

3. Conditional sampling methods and their generalizations

The basic methods and procedures for conditional analysis of plasma fluctuations have been described in detail elsewhere with references given before. The *interpretation* of the results depends basically on two seemingly different points of view. The strict analytical approach identifies the conditional average as the best estimate for the space-time evolution of the signal at times in an interval before and after the assumed condition has been fulfilled. This interpretation was suggested by Johnsen *et al* [2], who deduced phase space properties associated with the plasma variations observed. This interpretation applies for all signals, irrespective of the possible presence of long-lived coherent structures, in particular also for Gaussian noise. The error in the prediction can be estimated by the conditional reproducibility or the related

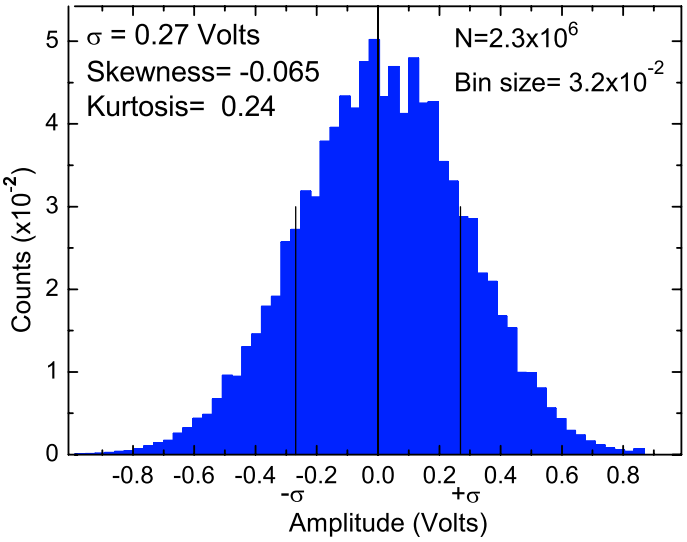

Figure 2. Amplitude distribution for the reference potential signal. The standard deviation is denoted σ. The values of skewness and kurtosis are inserted in the figure. The data are normalized to have unit sum.

conditional variance used by several authors [5, 8]. As to be expected, the uncertainty in the estimate will in general increase with increasing spatial as well as temporal separations from the space-time reference.

The conditional averaging analysis can also be seen as an approach to identify large coherent structures in a background of additive random noise. If such a dominant structure is present, the near future in the vicinity of the reference position will be mostly determined by the space-time evolution of that structure. Seen in this perspective, two basically different errors for identifying the structure can be found [12, 30]. We can experience that the local noise level exceeds the acceptance criterion, and gives a false event, unrelated to the presence of any large coherent structure. This can happen frequently if the amplitudes of the structures are comparable to the root mean square of the noise amplitude. In addition to this trigger error, a temporal 'jitter' of the triggering can occur, when the true value of the acceptance time is changed due to a noise component superimposed on the signal from the structure. This type of error can occur frequently even when the structures are large in amplitude. When averaging over all conditionally selected members of the sub-ensemble, the latter type of error will smear out the result, as compared to the ideal case where the occurrence of the structure is fixed with respect to the reference time given by the acceptance criterion. Another source of uncertainty arises in the case where the structures that might be present in the background noise have a distribution in one or more of the parameters, the amplitude for instance. The standard conditional average will have preference for detecting the largest ones. By elaborate methods, it is possible to obtain information on the distribution of some parameters, but this will be at the expense of a lengthy analysis [13].

One particular problem might be emphasized here. It is easy to visualize cases where the conditional average is not the best representation for the phenomena being studied, in particular when the random process is non-Gaussian. For instance for honest dice, we have the average outcome of counting the dots over many realizations to be $3\frac{1}{2}$, but this number of dots will

of course never occur! For cases which are significantly far from being Gaussian, it might be a better representation of the process to obtain the entire space-time varying conditional probability density, and then find its extremum value for varying r and t as illustrated by Johnsen *et al* [2]. (We can exemplify the meaning of conditions being far from Gaussian, by considering $\epsilon \equiv \int_{-\infty}^{\infty}(P(x)-G(x))^2\,\mathrm{d}x / \int_{-\infty}^{\infty} G^2(x)\,\mathrm{d}x$ with P being the probability density of the process and G being a Gaussian distribution with the same average and standard deviation. If $\epsilon \geqslant 1$ we might state that the process is far from being Gaussian. Similar arguments apply for multi-variable processes.)

3.1. Conditional sampling of Gaussian noise

We point out here that the standard form of a conditional analysis will always give *some* result, even when no coherent structures are present in the background noise [31]. For a Gaussian random process, for instance, the resulting average can be deduced from the correlation function of the signal one way or the other, since this function contains all the available information for that case [32, 33]. This property has been used to test for the Gaussian property of signals [34]. To illustrate this observation, we first determine the unconditioned estimate of the potential that minimizes the mean square error $e \equiv \langle(\hat{\phi}-\phi)^2\rangle$. Here $\hat{\phi}$ is the estimate, and ϕ the actual potential, assuming stationary time and locally homogeneous conditions here and in the following. We trivially find that the best estimate here is the average value $\hat{\phi} = \langle\phi\rangle$, and the error on the estimate is $e = \langle\phi^2\rangle - \langle\phi\rangle^2$.

If we have some *a priori* information, for instance given the potential at a certain reference time and position $(\mathbf{r}_0, t_0) = (0, 0)$ as ϕ_1, we can express the estimate as $\hat{\phi} = a + b\phi_1$ and determine a and b in such a way that the mean-square error is also minimized [7, 32]. In general, we have $a = a(\mathbf{r}, t)$ and $b = b(\mathbf{r}, t)$. Requiring that ϕ_1 is taken from the distribution of fluctuations in the system, we readily find that $\partial e/\partial a = 0$ and $\partial e/\partial b = 0$ when

$$\hat{\phi} = \langle\phi\rangle + \frac{\mathcal{R}(\mathbf{r}, t) - \langle\phi\rangle^2}{\langle\phi^2\rangle - \langle\phi\rangle^2}\,(\phi_1 - \langle\phi\rangle)\,, \tag{2}$$

where $\mathcal{R} \equiv \langle\phi(0)\phi(\mathbf{r}, t)\rangle$ is the correlation function for the potential, for spatial and temporal separations $\mathbf{r}$ and t. By proper choice of the potential reference we might achieve $\langle\phi\rangle = 0$. The foregoing results are correct for strictly Gaussian processes, and serve as the lowest order approximation in other cases as well [7, 32]. More general nonlinear estimates $\hat{\phi} = \sum_{n=0}^{\infty} a_n\phi_1^n$ can be introduced [32]. The fluctuations in the Blaamann plasma are non-Gaussian, as evidenced already by the one-point statistical distributions, see figure 2. (In principle one *might* find that the estimate of the one-point distribution is Gaussian to a good approximation, while the non-Gaussian features are manifested in the two-point, or higher, amplitude distributions.)

For a Gaussian random signal with zero mean, the error in the conditional estimator [33] is readily obtained as $e = \langle\phi^2\rangle - \mathcal{R}^2(\mathbf{r}, t)/\langle\phi^2\rangle$. For $\mathbf{r} = 0$ and time separations smaller than the micro-timescale, as determined by the curvature of the correlation function, we have $\mathcal{R}^2 \approx \langle\phi^2\rangle^2$, and the error is negligible. For time separations larger than the correlation time, the error approaches the unconditioned error $\langle\phi^2\rangle$ for all $\mathbf{r}$.

Assume now that we in error assume coherent structures to be present in a background of Gaussian random noise, and attempt to perform a filtering with an irrelevant filter. Even though the basic assumption is in error, we will nonetheless from time to time get a nontrivial filter output. In this case the maximum of the filter output occurs at a randomly distributed value for the reference signal, say ϕ_1, with some unknown distribution, $P(\phi_1)$. For each value of

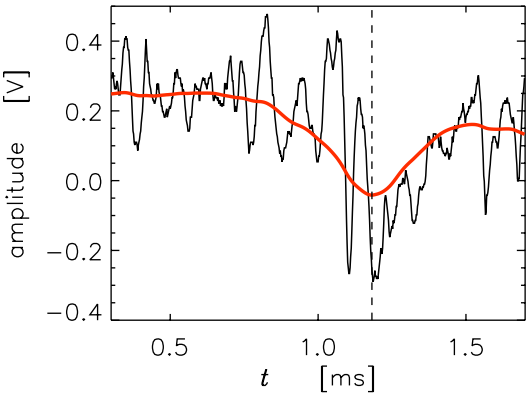

Figure 3. Selected data sample from the reference signal, showing the rapid oscillations superimposed on a slower sawtooth variation. Only a section of a longer signal is shown. The red curve shows the same signal sequence after application of the matched-filter (4). The filtered signal has a negative extremum when the structure is present since we took the filter amplitude to be positive in (4). The vertical dashed line indicates the reference time given for this particular case.

the potential in a narrow interval, $\phi \in \{\phi_1 : \phi_1 + \mathrm{d}\phi_1\}$, we have the result (2). By performing a conditioned ensemble average, we average over all ϕ_1 to obtain the estimate

$$\hat{\phi} = \frac{\mathcal{R}(\mathbf{r}, t)}{\langle \phi^2 \rangle} \int \phi_1 P(\phi_1)\, \mathrm{d}\phi_1, \tag{3}$$

where we for simplicity assumed $\langle \phi \rangle = 0$. Although we do not know $P(\phi_1)$, we find that again the space-time variation of the estimator for the conditionally averaged potential is determined by the correlation function, apart from a multiplicative constant. If the filter is wide compared to the correlation time of the noise, we will find $\int \phi_1 P(\phi_1)\, \mathrm{d}\phi_1 \approx 0$ giving $\hat{\phi} \approx 0$, while a narrower filter will give some finite value.

4. Methods for data analysis

In figure 3 we show a sample of data as obtained from the reference probe, which is detecting fluctuations in the floating potential. We can readily identify the rapidly oscillating component analyzed in previous works [5, 18]. In addition, we note a sawtooth-like variation of the signal, having a larger timescale and a typical amplitude of ∼0.5–1.0 V at the reference probe position. By simple inspection it is evident that the Fourier spectrum for the spiky structures is much wider than for the sawtooth variations.

Investigating many time sequences, we find that the sawtooth characteristics re-occur with seemingly random time intervals, with a random separation τ_S, where the average time separation is $\langle \tau_S \rangle \approx 4$ ms, with a scatter around this average being close to $\langle \tau_S \rangle$. The spiky component is, in comparison, much more regular, and gives a clear peak in the power spectrum of the fluctuations [5, 18], although the details of the power spectra can depend significantly on plasma parameters and other experimental conditions, such as neutral pressure and magnetic fields.

We decided to investigate whether the sawtooth-like phenomenon was a characteristic of the entire plasma column, or a localized effect of minor importance. For this purpose we designed a matched-filter having the optimum characteristic of the observed sawteeth. The remaining part of the signal is not white noise, but its spectral distribution is much wider than that of the sawtooth, so we anticipate that the suggested matched-filter is the best one. We let the filter be characterized by

$$f(\tau) = \begin{cases} (\tau + a)/a & \text{for} \quad -a < \tau < 0\,, \\ -(\tau - b)/b & \text{for} \quad 0 < \tau < b\,, \\ 0 & \text{for} \quad \tau < -a\,,\ \tau > b. \end{cases} \tag{4}$$

The absolute value of the maximum amplitude of f is irrelevant for a linear filter, and it is here set to unity. We have the two parameters $a > 0$ and $b > 0$ for optimizing the matching. The filter (4) contains our presumed knowledge of the phenomena being studied. In figure 3, we also show the signal sequence after filtering by a red line. The local maximum excursion of the filtered signal defines our reference time for the subsequent conditional sampling of the signal from the moving probe. Given a number of reference times found by this method, we subsequently average signals from the moving probe as before [5, 18], by selecting time sequences of the signals from the movable probe around the reference times. We note that the sawtooth phenomena are relatively rare, so the signal-to-noise ratio of the corresponding conditional average is not as good as for the case where the abundant spiky component is being analyzed. To improve the presentation we smooth the spatial variations in the final figures. We have no temporal averaging in the movie sample (available from stacks.iop.org/NJP/10/033030/mmedia).

Note that we can use the matched-filter output also to *exclude* time sequences from the analysis, i.e. analyze everything *but* the selected event! This procedure will for instance give a slight improvement of the signal-to-noise ratio of a conditional averaging of the spiky, more regular events.

4.1. Test of the method using synthetic data

In order to illustrate some details in the procedure of the analysis, we present also results using synthetic data [35]. The idea is to generate a signal by a random superposition of structures to generate a long time sequence for analysis [36]. Since we know exactly what the input has been, it is possible to test the performance of various methods, for instance also the modified conditional analysis outlined here. The time series is here generated by many randomly distributed wave packets added to a distribution of comparatively few triangular pulses, representing the crash. We do not aim at producing a signal emulating results like those in figure 3, merely illustrating its main features. The temporally varying signal is generated by a random superposition of some elementary structures, or wave packets $a\Psi(t)$, which, if needed, can be carefully tailored to reproduce all details of the power spectrum as well as the bispectrum of the background noise [35]. By this procedure we have $h(t) = \sum_{j=1}^{N} a\Psi(t - t_j)$, where t_j is a reference time of basic structure number j, and N is the (large) number of structures. For cases relevant here we take $\int_{-\infty}^{\infty} a\Psi(t)\,\mathrm{d}t = 0$, implying $\langle h(t)\rangle = 0$. It can be shown [36] that $\langle h^2(t)\rangle = \mu a^2 \int_{-\infty}^{\infty} \Psi^2(t)\,\mathrm{d}t$, with μ being the density of structures in the record. With T being the duration of the synthetic noise signal, it can be demonstrated that Gaussian noise is recovered in the limit $\mu = N/T \to \infty$, while $a \to 0$ in such a way that $aN/T = \text{const}$. The method for generating synthetic signals outlined here can be extended and generalized significantly [36].

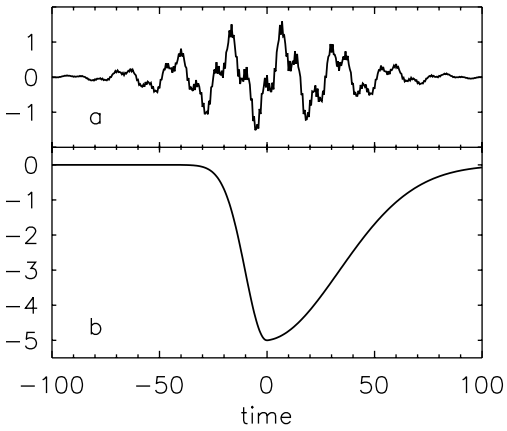

Figure 4. Basic structure used to generate the noise signal in (a), and the event representing a rapid potential drop and a slower recovery phase in (b). Times are in computational units.

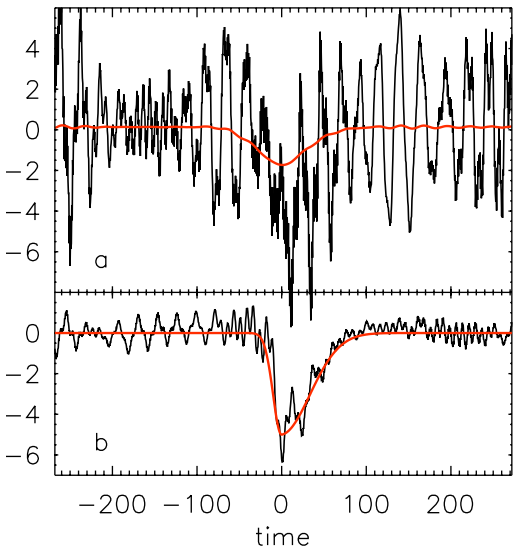

Figure 5. Sample of raw synthetic data, superposed on a crash are shown in (a). A red line gives the filter output with the maximum value chosen to be at the origin of the horizontal axis. In (b) we find the conditionally averaged signal for 50 events. A red line gives the time variation of the basic event from figure 4(b).

In figure 4 we show the basic structure used for generating the noise, and the triangular representation of a crash-like event. We are not attempting here to explore all details of the noise signal representation. We generate conditions which resemble those found in the experiment, i.e. we create a background 'spiky' noise, where $\sqrt{\langle h^2(t)\rangle}$ is approximately the same as the crash amplitude. We have here the standard deviation $\sigma = 3.0$ to be compared with an amplitude 5 of the triangular event in figure 4(b). We have a skewness $S = -0.31$ and a kurtosis $K = 0.2$.

The synthetic data are analyzed by the code used for analyzing the laboratory data. In figure 5 we show a sample of the noise signal superimposed on a crash-like event. With red

color we show the output of the filter, using the same analysis program used for analyzing the experimental data. Only a modest number of crashes (here 50) are included in the entire sequence, in order to mimic also the relatively rare occurrence of these events. These pulses have duration of ∼100 and are distributed over a time series of 10^5 in computational time units. We find that the matched filter recovers them all, and we have no false events for the conditions used here. Figure 5 also shows the conditional average obtained for these parameters. In spite of the relatively few events used here, we find the overall time variation of the crash to be faithfully reproduced.

The analysis of the real data based on triggers given by the output of the matched filter has, in general, also error sources such as false events and jitter as discussed in section 3, and the method can probably be fine-tuned just like the conditional analysis in its original version [12, 30]. For the synthetic signal discussed before, we did not find any false events and did not miss any true ones either. Small effects of jitter could be observed, but these were of little significance because the corresponding temporal uncertainty was of the order of the duration of a spike in the noise, which is much smaller than the triangular event being considered, see figures 4 and 5.

5. Experimental results

Using the outputs of the reference signal after filtering by the matched filter, we obtain a series of reference times, which are subsequently used for analyzing simultaneously recorded signals from the moving probe, as outlined before. We carry out two basically different investigations. The conditionally averaged potential is obtained, and also the local variations in fluctuation spectra are studied by use of a wavelet transform.

5.1. Conditionally averaged fluctuations

Results of the floating potential fluctuations derived by a matched filter-based conditional averaging are shown in figure 6 with a 16 μs time-resolution over the entire cross-section of the plasma. The time varying signals are to be understood as superimposed on the time averaged conditions shown in figure 1. In the example taken from the reference signal as shown in figure 3, the peak potential drop is ~ -0.5 V, but this peak value increases towards the center of the plasma profile. The events detected by the matched filter are relatively reproducible, so we obtain a good signal-to-noise level, in spite of the relatively few events observed (as compared with the results from a more standard conditional sampling).

By inspection of the results in figure 6, we note that starting with an asymmetric dipolar structure, the potential in the plasma drops or 'crashes' suddenly, within ∼50 μs, to be followed by a slow recovery phase, lasting in excess of ∼200 μs. The process happens almost simultaneously in the entire cross-section of the plasma, apart from a small region in the lower right of the figures, where the potential increases somewhat in a transient period. In particular, there is no rotation or motion otherwise associated with the observed potential variation. The oscillatory contribution seen in a single realization as figure 3 is absent from figure 6, indicating that the matched filter output is uncorrelated with the phase of these oscillations. In the movie, available from stacks.iop.org/NJP/10/033030/mmedia, we show the conditional potential evolution for an extended time period, noting that some irregularly moving smaller amplitude ripples preceded the crash.

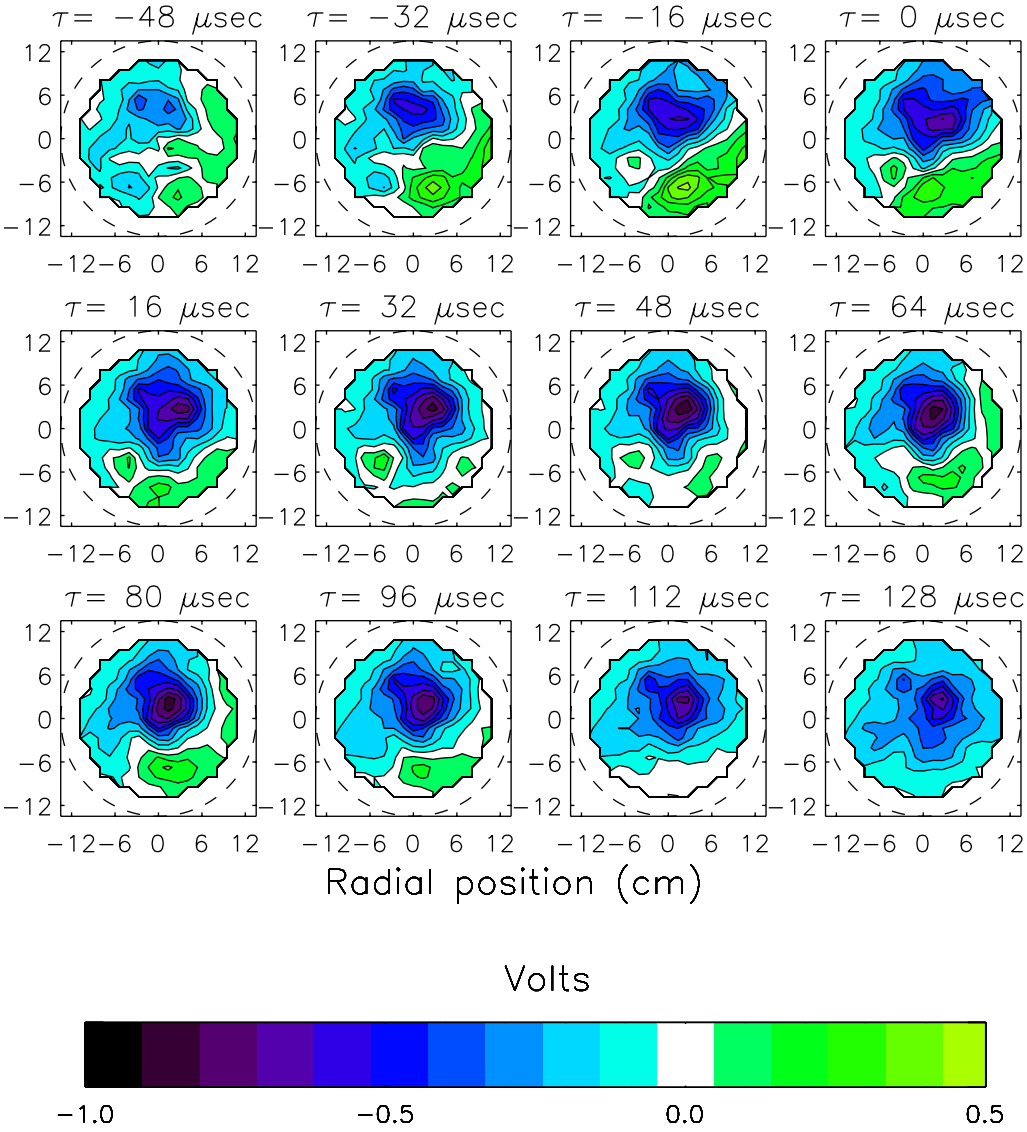

Figure 6. 2D contour plots of floating potential fluctuations derived by a matched filter-based conditional averaging. The temporal evolution starts at $-48\,\mu$s with respect to the reference times, and it is shown for every $16\,\mu$s up to $128\,\mu$s, see also the movie (available from stacks.iop.org/NJP/10/033030/mmedia) for an extended time interval. A white region is inserted to emphasize the zero level.

As a further illustration, we show in figure 7 an extended sequence of the time evolution of the conditionally averaged potential as detected at two positions close to the local minimum seen in figure 6. Recall here that figure 6, as well as the movie, rely on numerical interpolation of a fixed spatial grid. The steepest part of the initial evolution gives approximately the $\sim 50\,\mu$s time-constant found at the reference position, while we also here note the longer recovery time. A localized potential maximum is observed prior to the crash at ~ -0.2 ms. There is a slight difference in the time variations of the averaged potential at the center of the plasma column and at the reference probe position.

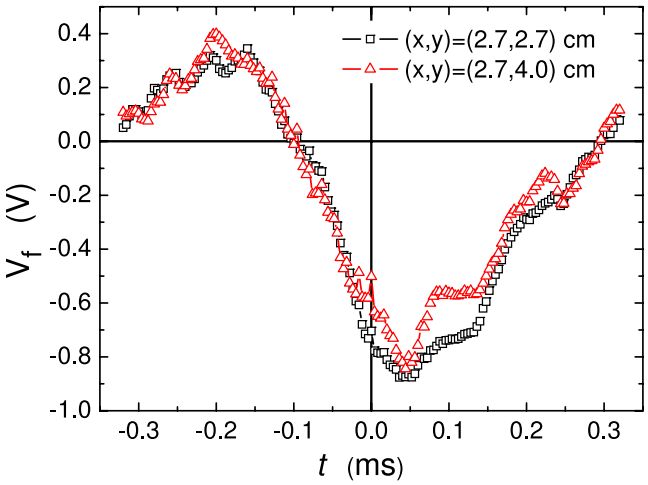

Figure 7. Time evolution of the conditionally averaged potential, as detected at two positions close to the minimum potential found on figure 6. The positions are marked on the insert.

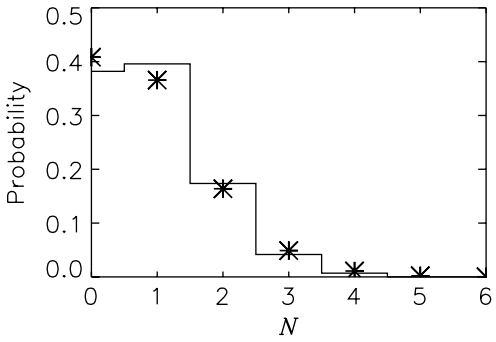

Figure 8. Distribution of the number of events, N, per 4.1 ms time intervals. Asterisks give the results obtained by a Poisson distribution, with the given average number of events $\langle N \rangle$. For the given conditions, $\langle N \rangle \approx 0.9$, which gives $\langle \tau_S \rangle \approx 4.5$ ms.

We have also analyzed the fluctuations in plasma density, finding only irregular variations in the plasma density during the potential crash itself, but we can also find significant precursors. The relative local variations in plasma density $\tilde{n}/\bar{n}(r)$ can be large in particular near the plasma edge, up to 0.3 ± 0.1.

With $\nabla^2\phi = e(n_e - n_i)/\varepsilon_0$, where $e > 0$, we note that the observed conditionally averaged potential in figure 6 has a positive curvature almost everywhere, corresponding to a net negative charge. We consequently find that the observed conditionally averaged potential variation is either due to selective loss of ions or intermittently enhanced confinement of the fast primary electrons.

5.2. Distribution of events

The temporal distribution of crash-events was analyzed by counting the number of identified events for the given duration of the time sequences, here 4.1 ms, analyzing a large number of

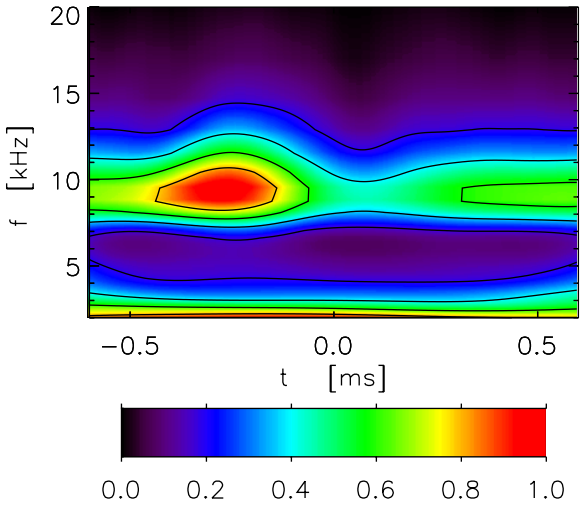

Figure 9. Conditioned power spectra obtained from the reference signal by using a wavelet transform, averaging more than 700 events. The spectrum is shown in linear color scale (in arbitrary units) for the range 2–20 kHz. The reference time is at $t = 0$. Only a part of an extended time sequence is shown.

such data sequences. The resulting distribution is shown in figure 8. In the case where crashes are statistically independent, we would expect them to follow a Poisson distribution [37], which is indicated by asterisks in figure 8. Overlap of crashes is rarely seen. The seemingly random temporal occurrence of crashes indicates that their origin is not a linear instability of the form discussed in section 2.2, i.e. interchange modes or potential relaxations.

5.3. Conditioned spectra

Every time the matched filter identifies an event, we take the local power spectrum of the reference signal by using a wavelet transform [38], using a Morelet mother wavelet. Many (more than 700) such conditional spectra are subsequently averaged. The results are shown in figure 9. The outer parts of the wavelet transform are influenced by edge effects, which extend also to low frequencies within the range shown. The shortest data time-sequences used are approximately 20% longer than the time interval shown. In principle, each spatial position in the plasma cross-section has a figure corresponding to figure 9, but we here show results only for the reference signal. These results are presented with a linear color code in arbitrary units, where the physical amplitude of the signals can be found in figure 3, for instance.

The basic and most important observation is that the local power spectrum is perturbed in the vicinity of the events detected by the matched filter. Prior to the crash, we note a clear enhancement of the local fluctuation level, followed by a void in the spectrum. Then, during the crash recovery phase, we again note an enhancement of the fluctuation intensity, although it is not quite as strong as in the crash phase. Ultimately, the fluctuations reach the average background level. By inspection of the single realization in figure 3, these features can be recognized, at least qualitatively. The crash and variation of the amplitude of the local power spectra are evidently correlated. The local enhancement of the fluctuations appears close to the local potential maximum seen in figure 7. The characteristic dominant frequency of the

background oscillations is close to the estimated plasma column rotation frequency $\Omega/2\pi$ found in section 2.1. The 9 kHz component may not properly be considered a wave-like disturbance, and it should rather be seen as an aperiodically unstable structure, propagating together with the bulk plasma motion. We also note a local enhancement of a low frequency component, around 2 kHz, accompanying the enhanced dominant 9 kHz component, but note that end effects influence the wavelet analysis at these low frequencies.

The *phases* of the fluctuations before and after the reference time given by the filter are random, consistent with observations mentioned in discussions of figure 6. If we first average the sin and cos parts of the Morelet wavelet transform, and *then* construct a power spectrum, we find a significant reduction in power.

It is not possible to tell from the observations alone what is the cause and effect of the amplitude variations observed, but the most reasonable assumption seems to be that the enhanced level of fluctuations gives rise to an anomalous transport of charged particles which subsequently causes the crash in potential.

It is interesting that the frequency of the fluctuations is approximately the same before, during and after the crash. By inspection of individual realizations we often find small 'glitches' or 'chirps' in the frequency spectrum, as also observed elsewhere [5]. The occurrence of these events is, however, not sufficiently frequent to make them noticeable in the averaged power spectra as shown in figure 9.

6. Conclusions

In the present study, we have generalized the standard method of conditional sampling as usually applied to electrostatic fluctuations in plasmas. The method of analysis was used for studying fluctuations in a toroidal magnetized plasma. Previous investigations of this plasma were concentrated on propagating coherent structures. By the generalized method, using a matched filter, we found new phenomena, consisting of a rapid 'crash' of the potential of the entire cross-section, followed by a slow recovery phase. Analyzing the plasma density variation by the same method, we found that the crash was preceded by large amplitude density fluctuations in a part of the plasma column. Within the crash we only find moderate amplitude, irregular oscillations in plasma density. A conditional wavelet analysis demonstrated that the power spectrum of the potential fluctuations had a local depletion associated with the events, with a small quiet time interval around the extremum of the sudden potential drop.

The present results should be compared with the standard analysis using the unfiltered reference signal. These results can be found in the literature, in particular for conditions like those studied here [18]. The most conspicuous difference can be found in the shorter timescales for the standard results and noting also that the structures usually observed [5, 18, 39] have an azimuthal propagation velocity, basically determined by the $\mathbf{E} \times \mathbf{B}$-velocity.

We also studied the distribution of events over time, obtaining evidence for a distribution being reasonably well represented by a Poisson distribution. Since a Poisson distribution applies for statistically independent events, we may argue that a viable model for the observed phenomena assumes that crashes appear independently, with equal probability of occurrence in any time interval of given length. The sole constraint seems to be that crashes should have marginal temporal overlap, at most.

We note a certain similarity between the signal shown in figure 3 and combined analytical–numerical results published in the literature [17]. One central difference is that the

sawtooth-like features there occur regularly. The analysis shows features having larger amplitudes as compared to those found in our study. This analysis [17] also demonstrates local variations in the power spectra, although details in the appearance are different from what we find here. It can thus not be argued that our present experimental results give solid support for the analytical results, but we nonetheless find the observed similarity interesting. The similarity might indicate that the crashes discussed in our study are induced by a rapid anomalous change in the charge distribution, where the enhanced fluctuations mediate this transport. Related studies [18] show a transient plasma burst towards the walls of the device using an analysis based on standard conditional averaging. It might be argued that these bursts can give rise to predominant loss of ions. The data analysis alone does not provide any evidence for the origin of the local amplitude of the oscillations, but it seems reasonable to assume a nonlinear mode coupling to be the origin. A possible candidate for the amplitude enhancement is the very low frequency $\sim$2 kHz oscillation barely noticeable in figure 9. The temporal localization of the wavelet analysis is poor at these low frequencies, and it is difficult to quantify the relative variations of the 9 kHz and the 2 kHz oscillations. An extended analysis is required to identify the origin of the crash and recovery phases found in this work, in particular their dependence on experimental parameters.

Evidently also the matched filter method for conditional averaging has its own limitations. Only little can be learned if the power spectrum of the structures is close to the power spectrum of the noise. Nonetheless, we believe that the results presented in the present work demonstrate that a dedicated pre-processing of the reference signal can give new and valuable results. In particular, we can imagine cases where a matched filter can be combined with other conditions in search of coherent structures in plasma and fluid turbulence.

Conditional averaging is an alternative to direct observations of individual coherent structures, which is after all also possible in some cases [40]. Direct observations will require that many probes are simultaneously present in the plasma. This can introduce unwanted disturbances.

Acknowledgments

The present datasets were obtained in the Blaamann device at the Auroral Observatory of the University of Tromsø. The experiment has now been dismantled on the request of the Norwegian National Science Foundation. We thank colleagues, students and technical staff for their contributions to the work on this experiment. In particular, we thank Terje Brundtland for his enthusiasm and tireless work in the construction and maintenance of the device.

References

[1] Blackwelder R F and Kaplan R E 1976 Wall structure of turbulent boundary-layer *J. Fluid Mech.* **76** 89–112
[2] Johnsen H, Pécseli H L and Trulsen J 1987 Conditional eddies in plasma turbulence *Phys. Fluids* **30** 2239–54
[3] Shapley A H and Beynon W J G 1965 Winter anomaly in the ionospheric absorption and stratospheric warmings *Nature* **206** 1242–3
[4] Huld T, Nielsen A H, Pécseli H L and Juul Rasmussen J 1991 Coherent structures in two-dimensional turbulence *Phys. Fluids* B **3** 1609–25
[5] Øynes F J, Olsen O-M, Pécseli H L, Fredriksen Å and Rypdal K 1998 Experimental study of low-frequency electrostatic fluctuations in a magnetized toroidal plasma *Phys. Rev.* E **57** 2242–55

[6] Antoni V, Drake J R, Spada E, Spolaore M, Vianello N, Bergsaker H, Cavazzana R, Cecconello M, Martines E and Serianni G 2006 Coherent structures and anomalous transport in reversed field pinch plasmas *Phys. Scr.* T **122** 1–7
[7] Pécseli H L and Trulsen J 1991 Analytical expressions for conditional averages: a numerical test *Phys. Scr.* **43** 503–7
[8] Nielsen A H, Pécseli H L and Rasmussen J J 1994 Experimental-evidence for mode selection in turbulent-plasma transport *Europhys. Lett.* **27** 209–14
[9] Grulke O, Klinger T and Piel A 1999 Experimental study of the dynamics of conditionally averaged structures in weakly developed electrostatic turbulence *Phys. Plasmas* **6** 788–96
[10] Roman H E 2007 Two-dimensional signal reconstruction: the correlation sampling method *Rev. Sci. Instrum.* **78** 123502
[11] Block D, Teliban I, Greiner F and Piel A 2006 Prospects and limitations of conditional averaging *Phys. Scr.* T **122** 25–33
[12] Teliban I, Block D, Piel A and Greiner F 2007 Improved conditional averaging technique for plasma fluctuation diagnostics *Plasma Phys. Control. Fusion* **49** 485–97
[13] Kofoed-Hansen O, Pécseli H L and Trulsen J 1989 Coherent structures in numerically simulated plasma turbulence *Phys. Scr.* **40** 280–94
[14] Turin G L 1960 An introduction to matched-filters *IRE Trans. Inf. Theory* **6** 311–29
[15] Mohanty N 1986 *Random Signal Estimation and Identification Analysis and Applications* (New York: Van Nostrand Reinhold)
[16] Rypdal K, Grønvoll E, Øynes F, Fredriksen Å, Armstrong R J, Trulsen J and Pécseli H L 1994 Confinement and turbulent transport in a plasma torus with no rotational transform *Plasma Phys. Control. Fusion* **36** 1099–114
[17] Rypdal K, Garcia O E and Paulsen J-V 1997 Anomalous cross-field current and fluctuating equilibrium of magnetized plasmas *Phys. Rev. Lett.* **79** 1857–60
[18] Fredriksen Å, Riccardi C, Cartegni L and Pécseli H 2003 Coherent structures, transport and intermittency in a magnetized plasma *Plasma Phys. Control. Fusion* **45** 721–33
[19] Rypdal K and Ratynskaia S 2006 Plasma profiles, waves and anomalous transport in a purely toroidal plasma modified by a biased internal anode *Phys. Scr.* T **122** 52–65
[20] Fredriksen Å, Riccardi C and Magni S 2006 Effects of edge dc biasing on plasma rotation and transport in a toroidal geometry *Phys. Scr.* T **122** 11–4
[21] Pécseli H L 1982 Drift-wave turbulence in low-β plasmas *Phys. Scr.* T **2A** 147–57
[22] Mikkelsen T and Pécseli H L 1980 Strong turbulence in partially ionized plasmas *Phys. Lett.* A **77** 159–62
[23] Odajima K 1978 Effects of radial electric-field on drift wave instability in a weakly ionized plasma *J. Phys. Soc. Japan* **44** 1685–93
[24] Rypdal K and Ratynskaia S 2004 Statistics of low-frequency plasma fluctuations in a simple magnetized torus *Phys. Plasmas* **10** 2686–95
[25] Greiner F, Block D and Piel A 2004 Observation of mode like coherent structures in curved magnetic fields of a simple magnetized torus *Contrib. Plasma Phys.* **44** 335–46
[26] Rogister A and D'Angelo N 1970 Type II irregularities in the equatorial electrojet *J. Geophys. Res.* **75** 3879–87
[27] D'Angelo N, Pécseli H L and Petersen P I 1974 Farley instability—a laboratory test *J. Geophys. Res.* **79** 4747–51
[28] Iizuka S, Michelsen P, Rasmussen J J, Schrittwieser R, Hatakeyama R, Saeki K and Sato N 1982 Dynamics of a potential barrier formed on the tail of a moving double-layer in a collisionless plasma *Phys. Rev. Lett.* **48** 145–8
[29] Klinger T and Piel A 1992 Investigations of attractors arising from the interaction of drift waves and potential relaxation instabilities *Phys. Fluids* B **4** 3990–5
[30] Block D, Teliban I and Piel A 2007 Experimental comparison of statistical and spatio-temporal probe diagnostics *Plasma Phys. Control. Fusion* **49** 1707–18

[31] Filippas A V, Bengston R D, Li G X, Meier M, Ritz C P and Powers E J 1995 Conditional analysis of floating potential fluctuations at the edge of the Texas experimental tokamak upgrade (TEXT-U) *Phys. Plasmas* **2** 839–45
[32] Adrian R J 1979 Conditional eddies in isotropic turbulence *Phys. Fluids* **22** 2065–70
[33] Edwards R V and Skov Jensen A 1983 Particle-sampling statistics in laser anemometers—sample-and-hold systems and saturable systems *J. Fluid Mech.* **133** 397–411
[34] Pécseli H L, Primdahl F and Bahnsen A 1989 Low-frequency electrostatic turbulence in the polar cap E region *J. Geophys. Res.* **94** 5337–49
[35] Pécseli H L and Trulsen J 1993 On the interpretation of experimental methods for investigating nonlinear wave phenomena *Plasma Phys. Control. Fusion* **35** 1701–15
[36] Rice S O 1944 Mathematical analysis of random noise I *Bell System Tech. J.* **23** 282–332
Reprinted by Wax N 1954 *Selected Papers on Noise and Stochastic Processes* (New York: Dover)
[37] Hogg R V and Craig A T 1970 *Introduction to Mathematical Statistics* 3rd edn (Indianapolis, IN: Macmillan)
[38] Mallat S 1998 *A Wavelet Tour of Signal Processing* (San Diego, CA: Academic)
[39] Fredriksen Å, Riccardi C, Cartegni L, Draghi D, Trasarti-Battistoni R and Roman H E 2003 Statistical analysis of turbulent flux and intermittency in the nonfusion magnetoplasma Blaamann *Phys. Plasmas* **10** 4335–40
[40] Zweben S J *et al* 2006 Structure and motion of edge turbulence in the national spherical torus experiment and Alcator C-mod *Phys. Plasmas* **13** 056114